

Effect of Oversized Factor on 0.1 THz Surface Wave Oscillator^{*})

Yuta ANNAKA, Kazuo OGURA¹⁾, Mao AOKI¹⁾, Shingo HAMADA¹⁾,
Tsubasa KATO¹⁾ and Masaya ITO¹⁾

Faculty of Engineering, Niigata University, Niigata 950-2181, Japan

¹⁾*Graduated School of Science and Technology, Niigata University, Niigata 950-2181, Japan*

(Received 7 January 2022 / Accepted 23 February 2022)

Surface wave oscillator (SWO) is an intense subterahertz wave source based on the interaction of an electron beam with a surface wave in a cylindrical corrugated waveguide (CCW). The oversized factor is a key parameter of SWO and is the ratio of the CCW diameter to the wavelength of a generated wave. In this study, we experimentally examine 0.1 THz SWO with different oversized factors of 10 and 7. For an oversized factor of 7, a kilowatt class radiation with a maximum efficiency of 8% is observed. SWO operation can be improved by decreasing the factor from 10 to 7.

© 2022 The Japan Society of Plasma Science and Nuclear Fusion Research

Keywords: surface wave oscillator, oversized factor, intense terahertz radiation, electron beam device

DOI: 10.1585/pfr.17.2406036

1. Introduction

An electron beam device has been proposed as an intense terahertz wave source [1]. A surface wave oscillator (SWO) is one of the electron beam devices based on the beam interaction with a surface wave. The SWO requires a 1 T order external magnetic field, which decreases the device cost and miniaturizes SWO to desk-top size. The subterahertz SWO has improved in recent experimental studies [2,3]. With the external magnetic field of 0.8 T, 0.1 THz SWO achieves a kilowatt class radiation and a 1% order efficiency according to Ref. [2]. In Ref. [3], N. S. Ginzburg et al. reported 150 MW radiation from 90 GHz 2D SWO with 3 T. The efficiency of this 2D SWO is larger than 10%. Despite this improvement, the performance of SWO is still lower than that of other electron beam devices such as gyrotron. For example, 300 GHz gyrotron achieves 320 kW radiation and an efficiency of 30% with an external magnetic field of 11.59 T [4]. Further studies are required for realizing compact high-power electron beam devices with a low external magnetic field.

In SWO, an oversized cylindrical corrugated waveguide (CCW) is often used to form a surface wave. The diameter D of the CCW is several times larger than the wavelength λ of the generated wave to generate high-power radiation [5]. The diameter to the wavelength is called the oversized factor, a key parameter of SWO for intense radiation. When the wavelength is millimeter order or less in terahertz frequency, the oversized factor tends to become too large. In Ref. [6], 0.3 and 0.4 THz CCWs have oversized factors of 30 and 40, respectively. The kilowatt class radiation with an efficiency of 0.01% order is obtained using these CCWs. The efficiency is lower than the 1% order

of the 0.1 THz SWO with an oversized factor of 10. In this regard, there is a desire for adequate oversized factors for terahertz SWO.

In this study, we experimentally examine 0.1 THz SWO with different oversized factors. The factor is adjusted by changing the diameter of the CCW, and the effect of the factor on SWO operation is investigated.

2. Analysis of Corrugated Waveguide

Figures 1 (a) and (b) show a schematic and an image of 0.1 THz CCW, respectively. The CCWs are made of aluminum and with corrugated inner walls. The corrugated wall is spatially periodic in an axial direction. In Fig. 1 (a), R is the radius of CCW, h is the amplitude of the structure, z_0 is a periodic length, and d is the width of a groove. These parameters are shown in Table 1. The image in Fig. 1 (b) shows 0.1 THz CCWs with $R = 14.85$ and 10.0 mm.

The dispersion relations of waveguide modes are calculated using a field-matching method to obtain the oversized factor of CCW [7]. Figure 2 (a) shows dispersion curves of TM_{01} fundamental waveguide modes with various radii R . Here, the vertical and horizontal axes represent the frequency and axial wavenumber of k_z , respectively. The dispersion curves are periodic with a period of $k_0 = 2\pi/z_0 = 125.66 \text{ cm}^{-1}$ and an upper cutoff appears at $k_z = 0.5k_0$ because of the spatial periodicity of the corrugated wall. In this study, the frequency determines the oversized factor at the upper cutoff. As the radius increases, the frequency decreases, and the oversized factor increases. Figure 2 (b) shows the dependence of frequency and oversized factors on the radius of CCW. The factor appears to be proportional to the radius because the wavelength variations are negligibly small compared with the radius.

author's e-mail: annaka@eng.niigata-u.ac.jp

^{*}) This article is based on the presentation at the 30th International Toki Conference on Plasma and Fusion Research (ITC30).

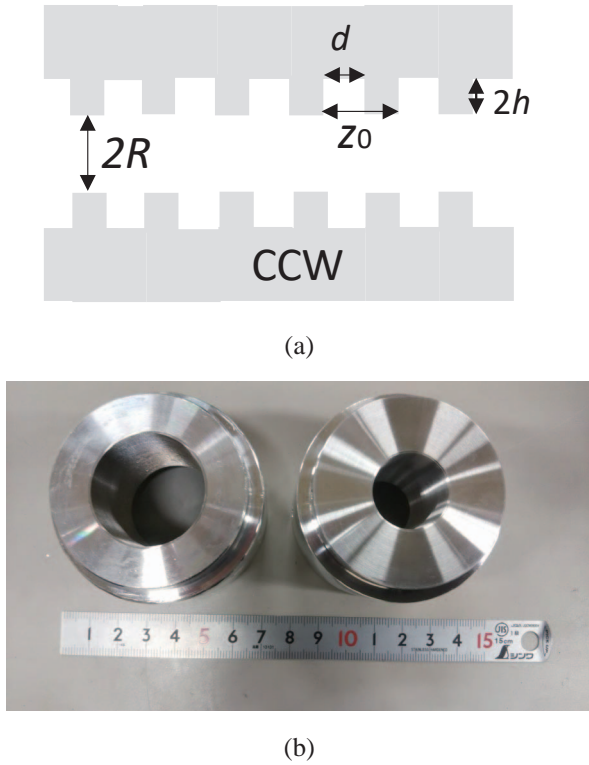


Fig. 1 (a) Schematic of CCW. (b) Image of 0.1 THz CCW with radiuses of $R = 14.85$ mm (left) and 10.0 mm (right).

Table 1 Size parameters of CCW.

h	d	z_0
0.3 mm	0.3 mm	0.5 mm

The oversized factors for the CCWs in Fig. 1 (b) are 10 for $R = 14.85$ mm and 7 for $R = 10.0$ mm. When the phase velocity $v_{ph} = \omega/k_z$ is slower than the velocity of light, a waveguide mode becomes a surface wave localized to the surface of the corrugated wall. The thin solid lines indicate light lines $\omega = ck_z$ and $\omega = -c(k_z - k_0)$, where ω is an angular frequency. The dashed line in Fig. 2 (a) shows the electron beam line with a beam energy of 20 keV and zero beam current. The slope of the beamline is the velocity of the electron beam. The surface wave would be excited around the intersection between the dispersion curve of the surface wave and the beam line. At the intersection, the surface wave has a negative group velocity and acts as negative feedback, which causes intense radiation.

3. Experiments

To examine the effect of the oversized factor, we conduct SWO experiments using two CCWs with the factors 10 and 7 in Fig. 1 (b). Figure 3 shows the schematic of the experimental setup. The setup is composed of an electron beam source and CCW in a vacuum chamber. The electron beam source is a set of a disk-type cold cathode and

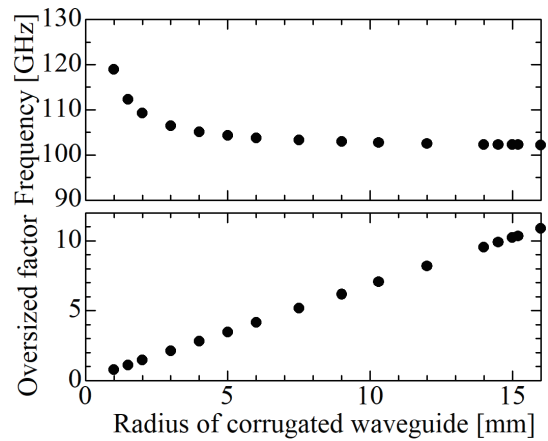
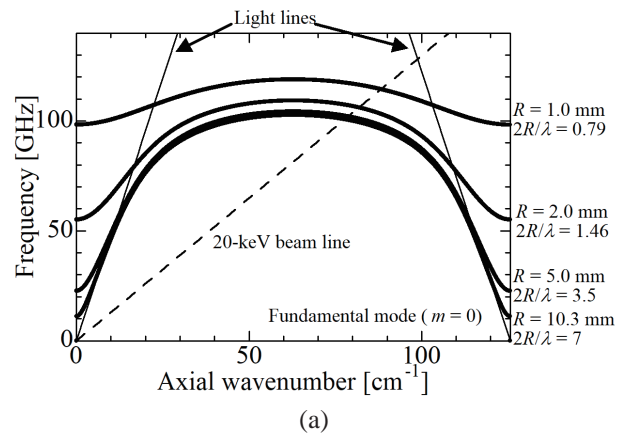


Fig. 2 (a) Dispersion relations of fundamental surface wave modes with $m = 0$ with various radius R . (b) Dependences of frequency at $k_z = 0.5k_0$ and oversized factor on radius of CCW.

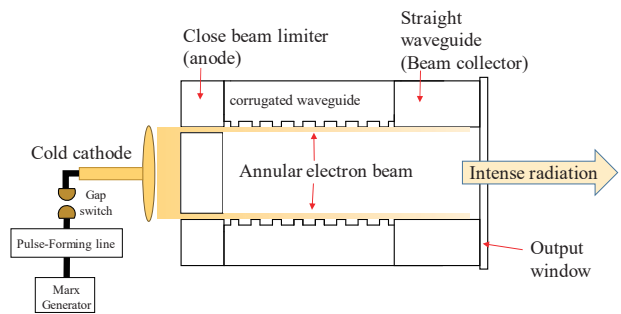


Fig. 3 Experimental setup of SWO.

beam limiter as an anode [8]. The diameters of the cathode and anode are chosen based on the radius R of the CCW. In this experiment, the cathode diameters are 29.5 mm for $R = 14.85$ mm, and 20.0 mm for $R = 10.0$ mm. The anode diameters are the same as the diameters of the CCWs. The anodes developed in Ref. [2] with close beam limiters are used. The close beam limiter restricts the current and width of an electron beam. The voltage supply, consisting of a Marx generator and pulse-forming line, is connected

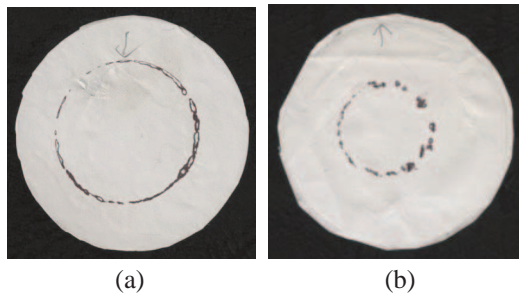


Fig. 4 Forms of electron beams printed on thermal papers with beam sources for oversized factors of (a) 10 and (b) 7.

to the cathode via a gap switch. A voltage up to 100 kV is applied to the cathode, and then an annular electron beam is generated. The beam is guided by an external magnetic field of 0.8 T generated by 10 solenoidal coils. The Rogowski coil measures the beam current. A surface wave in the CCW is excited by the electron beam, and the exciting surface wave is converted into a volume wave in a cylindrical straight waveguide connected to the CCW. The straight waveguide has the same radius as CCW. As the beam collector, the electron beam is absorbed by the wall of the straight waveguide. The volume wave is radiated from an output window. The window is made of Teflon with a width of 10 mm. The transmission rate of the window is measured using a 100 GHz Gun diode and is 72%.

The forms of the electron beams are examined by printing them on thermal papers in Fig. 4. The radiuses of the annular beams correspond to that of the beam limiter. The radial thicknesses are not uniform and are within 1 mm.

The radiated wave from the window is observed by detecting systems with frequency bands F-band and G-band. The system is composed of a horn antenna, a rectangular waveguide, an attenuator, and a crystal diode detector. The cutoff frequencies of F-band and G-band are 74 and 116 GHz, respectively. The horn antennas were located 600 mm from the output window.

Figure 5 shows the cathode voltage, beam current, and observed signals of F-band and G-band detectors. F-band signal is observed with a 30 dB attenuator. The cathode voltage reached a peak value of 28 kV at 170 ns and began to decrease from 170 ns. The F-band signal peaks at 285 ns with the cathode voltage of 19.9 kV and beam current of 1.7 A. There was no meaningful signal observed using a G-band detector with a cutoff frequency of 116 GHz and no attenuator. The cutoff frequencies imply that the frequency of the observed wave is in the range of 74 to 116 GHz. This frequency range includes the frequency of the surface wave with an oversized factor of 7. The excitation of the surface wave would generate the observed signal.

Figure 6 shows the dependence of F-band observed powers with the factors of 7 and 10 on the cathode voltage. The maximum-observed power is 2.6 W for the oversized

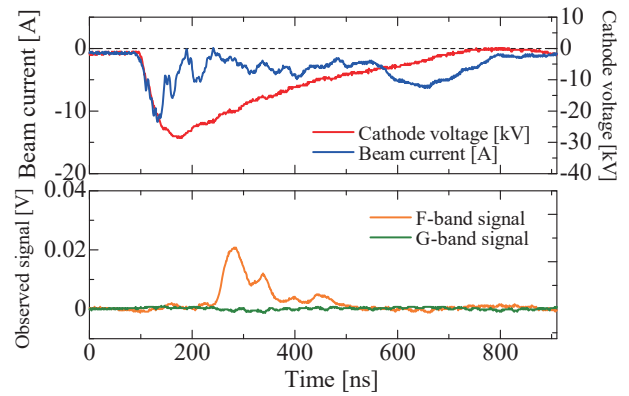


Fig. 5 Cathode voltage, beam current, and observed signals of F-band and G-band detectors with oversized factor of 7.

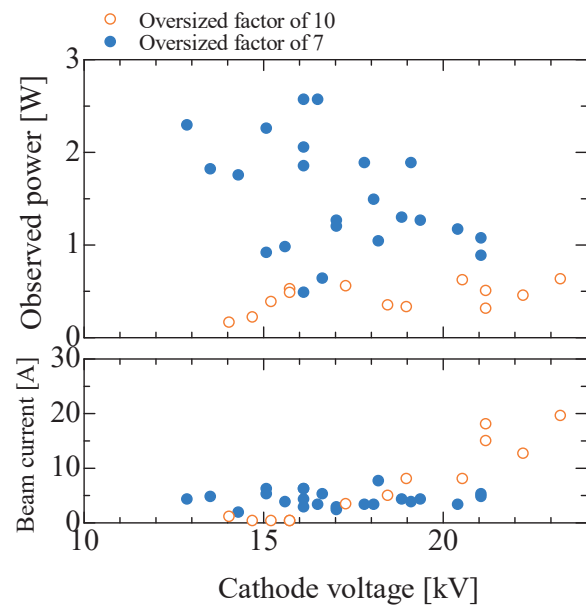


Fig. 6 Dependences of F-band observed power and beam current on cathode voltage.

factor of 7, whereas that is less than 1 W for 10. The observed power increases as the factor decreases from 10 to 7. The total power of the radiated wave is examined using the radiation pattern measurement. By changing the position of the horn antenna from -40° to 40° , the radiation pattern for the oversized factor of 7 is obtained, as shown in Fig. 7. The plots indicate an average value of five shots. The average voltage and current are 14.8 kV and 2.7 A, respectively. The solid lines are calculated radiation patterns for TM_{01} and nonaxisymmetric modes with azimuthal mode numbers of $m = 6$ and 10 [9]. The radiation pattern extends from -40° to 40° , and the peaks appear at approximately $\pm 5^\circ$, which correspond to TM_{01} mode. This implies that the generated radiation includes multimode up to $m = 10$, and the TM_{01} ($m = 0$) mode is dominant. The total radiation power is estimated by integrating patterns from -40° to 40° and is 2 kW. The efficiency is 5%, which

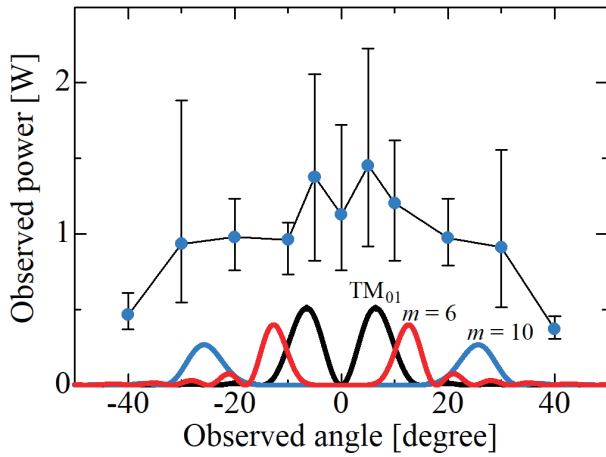


Fig. 7 Radiation pattern for oversized factor of 7 in range of observed angle from -40° to 40° .

is the ratio of the total radiation power to the input power of the electron beam.

4. Discussion and Conclusion

In this study, we examine 0.1 THz SWO with different oversized factors. The kilowatt class radiation with an efficiency of 5% is obtained with an oversized factor of 7. The efficiency with the factor of 7 is higher than that of 10 according to Refs. [2, 10]. There are two possible explanations for the improved efficiency. First, the density of the electron beam would change the radiation power. The beam diode for the factor of 7 generates an annular electron beam whose radius is smaller than that for the factor of 10. The density of the electron beam increases as the radius gets smaller. An electron beam with a high density would improve SWO operation. Second, a sparse-mode spectrum allows for mode competition to be avoided [3]. Figure 8 shows the dependence of the frequencies at $k_z = 0.5k_0$ with the factors of 7 and 10 on the azimuthal mode number m . The plotted values are obtained from the dispersion curves calculated using the field-matching method. The dispersion curve of the surface wave can be expressed as

$$\left(\frac{\omega}{c}\right)^2 = \left(\frac{\omega_0(k_z)}{c}\right)^2 + \left(\frac{m}{R}\right)^2. \quad (1)$$

Here, $\omega_0(k_z)$ is the dispersion relation of the TM_{01} mode as those in Fig. 2(a). The spatial periodicity in Fig. 1(a) varies the radius r along the z -direction and relates the radial and axial wavenumbers, resulting in the dispersion curve $\omega_0(k_z)$. Nevertheless, θ remains an independent variable in the CCW, and the azimuthal wavenumber $k_\theta = m/R$ is independent of k_z and k_r , leading to Eq. (1). The dashed lines in Fig. 8 represent Eq. (1), which corresponds to the plotted values. The radius R decreases as the second term on the right side of Eq. (1) increases with the mode number m . With $m = 22$ for the oversized factor of 7 and with $m = 31$ for the factor of 10, the second term becomes al-

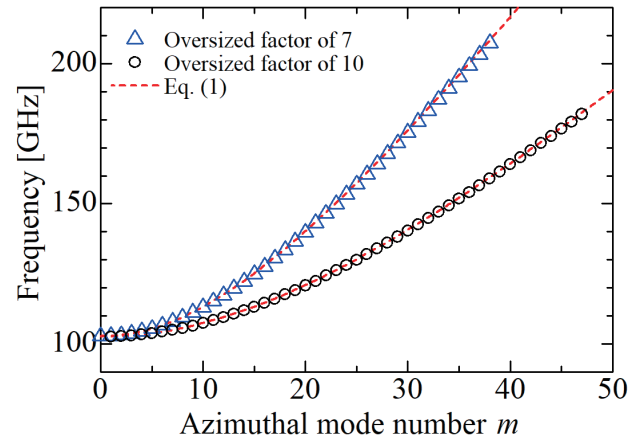


Fig. 8 Dependences of frequency of surface wave at $k_z = 0.5k_0$ with oversized factors of 7 and 10 depending on azimuthal mode number m .

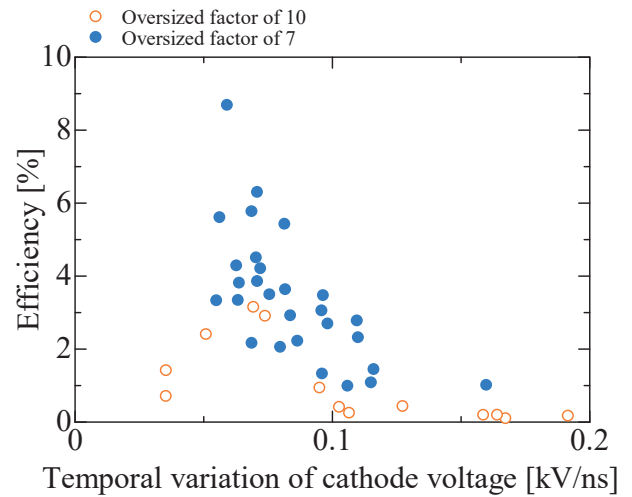


Fig. 9 Dependences of efficiency on temporal variation of cathode voltage.

most the same as the first term. The mode spectrum becomes sparse with the second term. The excitable modes decrease with the sparse spectrum, and then the effect of the mode competition would decay.

The efficiency of 5% is obtained from the average radiation powers plotted in Fig. 6. The ratio of the total power to the observed power is 1300, which is roughly estimated from Fig. 7. Then, the efficiency is obtained from the observed power in Fig. 6, and the maximum efficiency is 8% for an oversized factor of 7. A time-integrated efficiency is obtained and the efficiency is at the peak. In Fig. 5, the radiation power, cathode voltage, and beam current are integrated from 240 to 360 ns, and then the integrated efficiency of 3.7% is obtained. It is 0.56 times the efficiency at the peak of 6.5%.

Figure 9 shows the dependence of the efficiency at the peak on the temporal variation of the cathode voltage. The maximum efficiency is obtained with approxi-

mately 0.06 kV/ns, and as the temporal variation increases, efficiency decreases. The interaction between the electron beam and the surface wave would be disrupted if there was too much temporal variation.

In Fig. 5, the beam current has peaks at approximately 130 and 650 ns. No meaningful F-band signal is seen at 130 and 650 ns although the signal is obtained with a lower current approximately 285 ns. The temporal variation of the cathode voltage at approximately 130 ns is larger than that at approximately 285 ns. Figure 9 shows that the large temporal variation degrades device performance. Hence, no meaningful signal is obtained at approximately 130 ns. The cathode voltage at approximately 650 ns is lower than 6 kV. Such a low voltage does not satisfy the starting conditions of the voltage [11].

In Fig. 6, the variation of the plotted value of the oversized factor of 7 is larger than that of the factor of 10. The power would be affected by the temporal variation of the cathode voltage and the quality of the electron beam. The performance of SWO depends on the temporal variation, which ranges from 0.04 to 0.2 kV/ns as shown in Fig. 9. Meanwhile, the beam form in Fig. 4 (b) is rougher than that in (a). The beam quality of (b) would be lower than (a) and then causes the larger variation of the plotted value in Fig. 5. Furthermore, the electron emission from the cold cathode used in this experiment is more unstable than that from a hot cathode and would result in low reproducibility of the beam quality.

The waveform of the beam current for the oversized factor of 7 in Fig. 5 is different from that for the factor of 10. The waveform for the factor of 10 appears as a rectangular pulse similar to Fig. 6 (a) of Ref. [2]. The quality of the beam may cause a difference in the waveform.

The radius of CCW would be 1 mm order when considering a terahertz SWO with the factor of 7. Such a small radius would cause manufacturing difficulties [12]. A rod-type corrugation may be suitable for the terahertz SWO rather than CCW [11].

In this study, we conduct experiments with the oversized factors of 7 and 10. The 100 GHz CCW with the lower factor does not examine because of manufacturing difficulties. However, the effect of the oversized factor would be compared with CCW in a different frequency band. The experiments with K-band and Q-band CCWs were conducted according to Ref. [13]. Those CCWs have the factors of 2.4 (K-band) and 4 (Q-band). The efficiencies are 1.8% for K-band and 1.1% for Q-band and are the same order of 100 GHz SWO with the factor of 10.

The performance of SWO is influenced by the width of the electron beam. The width in this study is within

1 mm, which is greater than the decay length of the surface wave from the corrugated wall [2]. The performance may be improved by decreasing the width. The appropriate width of the beam will be examined in our future work.

Other than the excitation of the surface wave, SWO has generation mechanisms including Orotron radiation and Smith-Purcell (SP) radiation [14]. Orotron radiation and SP radiation occur based on the beam interaction with the fast wave with a phase velocity faster than the speed of light. In this study, no Orotron and SP radiations were observed because the frequency of the observed radiation is in the range from 74 to 116 GHz, and the electron beam interacts with the fast waves above 116 GHz.

In conclusion, we demonstrate that the subterahertz SWO is improved by adjusting the oversized factor. The adjusted factor realizes a high-performance subterahertz SWO with less than 1 T external magnetic field.

This work has been partially supported by JSPS KAKENHI Grant Number 20K15191.

- [1] S.S. Dhillon *et al.*, *J. Phys. D: Appl. Phys.* **50**, 043001 (2017).
- [2] Y. Annaka, K. Ogura, Y. Sato and M. Nakasone, *Jpn. J. Appl. Phys.* **59**, SHHD02 (2020).
- [3] N.S. Ginzburg, V. Yu. Zaslavsky, A.M. Malkin, A.S. Sergeev, I.V. Zotova, K.A. Sharypov, S.A. Shunailov, V.G. Shpak, M.R. Ul'masculov and M.I. Yalandin, *Appl. Phys. Lett.* **117**, 183505 (2020).
- [4] T. Saito, Y. Yamaguchi, Y. Tatematsu, M. Fukunari, T. Hirobe, S. Tanaka, R. Shinbayashi, T. Shimozuma, S. Kubo, K. Tanaka and M. Nishiura, *Plasma Fusion Res.* **12**, 1206013 (2017).
- [5] K. Ogura, K. Komiyama, M. Sakai, D. Yamada, H. Saito and H. Yamazaki, *IEEE Trans. FM* **125**, 733 (2005).
- [6] M.T. San, K. Ogura, K. Kubota, Y. Annaka, K. Yambe and A. Sugawara, *IEEE Trans. Plasma Sci.* **46**, 530 (2018).
- [7] K. Ogura, Y. Annaka, Y. Hoshi and T. Takahashi, *IEEE Trans. Plasma Sci.* **49**, 40 (2021).
- [8] K. Yambe, K. Ogura, S. Hasegawa, T. Shinada, T. Iwasaki and T. Furuichi, *IEEE Trans. Plasma Sci.* **41**, 2781 (2013).
- [9] S. Silver, *Microwave Antenna Theory and Design*, Chap. 10 (McGRAW-HILL BOOK COMPANY, 1949).
- [10] M. Aoki, Y. Annaka, K. Ogura and M. Ito, *Jpn. J. Appl. Phys.* **60**, 096004 (2021).
- [11] S. Gong, K. Ogura, K. Yambe, S. Nomizu, A. Shirai, K. Yamazaki, J. Kawamura, T. Miura, S. Takashi and M.T. San, *J. Appl. Phys.* **118**, 123101 (2015).
- [12] Y. Annaka, K. Ogura, K. Rachi, Y. Hoshi, S. Kubo, T. Shimozuma, S. Kobayashi and K. Okada, *IEEE Trans. Plasma Sci.* **49**, 33 (2021).
- [13] S. Aoyama, Y. Miyazawa, K. Ogura, A. Sugawara and M. Hirata, *Fusion Sci. Technol.* **51**, 325 (2007).
- [14] Y. Annaka, K. Ogura, K. Ozawa, K. Sekine and M.T. San, *Phys. Plasma* **25**, 063115 (2018).